ELSEVIER

Journal of Magnetism and Magnetic Materials 214 (2000) 13–30

Journal of magnetism and magnetic materials

www.elsevier.com/locate/jmmm

Structural and magnetic studies on heavy-metal-adsorbing iron sulphide nanoparticles produced by sulphate-reducing bacteria

J.H.P Watson[a,*], B.A. Cressey[b], A.P. Roberts[b], D.C. Ellwood[a], J.M. Charnock[c], A.K. Soper[d]

[a]*Department of Physics and Astronomy, University of Southampton, Southampton SO17 1BJ, UK*
[b]*School of Oceanographic and Earth Sciences, University of Southampton, Southampton SO14 3ZH, UK*
[c]*Daresbury Laboratory, Daresbury Warrington, Cheshire WA4 4AD, UK*
[d]*ISIS Facility, Rutherford-Appleton Laboratory, Chilton Didcot, Oxfordshire OX11 0QX, UK*

Received 12 October 1999; received in revised form 23 December 1999

Abstract

In previous and in work to be published, it has been shown that iron sulphide material, produced by sulphate-reducing bacteria (SRB), is an excellent adsorbent for a wide range of heavy metals. The material adsorbs between 100 and 400 mg g^{-1} and residual levels in solutions can be of the order of pg per litre. Further, strongly magnetic forms of this material can now be produced which can be effectively and cheaply removed from suspension together with the adsorbate by magnetic separation. This paper examines the structure of weakly magnetic and strongly magnetic iron sulphide material produced by SRB with a view to increasing the understanding of its adsorbent and the magnetic properties. The structural properties have been examined using high-resolution imaging and electron diffraction in a transmission electron microscope (TEM), the measurements of magnetisation versus field and temperature, extended X-ray absorption fine-structure (EXAFS) spectroscopy, X-ray absorption near-edge structure (XANES) spectroscopy and neutron diffraction. Before drying the surface area of both the weakly magnetic and the strongly magnetic iron sulphide is of the order of 400–500 m^2 g^{-1} as revealed by the magnetic properties, neutron scattering and the adsorption of a number of heavy metals. After freeze-drying the surface area falls to between 18 and 19 m^2 g^{-1}. The initial inocula came from a semi-saline source and when fed with nutrient containing Fe^{2+} and Fe^{3+} produced a weakly magnetic iron sulphide (Watson et al., Minerals Eng. 8 (1995) 1097) and a few % of a more strongly magnetic material. Further work using a novel method (Keller-Besrest, Collin, J. Solid State Chem. 84 (1990) 211) produced a strongly magnetic iron sulphide material. EXAFS and XANES spectroscopy revealed (Keller-Besrest and Collin, 1990) that the weakly magnetic iron sulphide material had the Ni–As structure in which the Fe is tetrahedrally coordinated with the composition $Fe_{1-x}S$. The strongly magnetic iron sulphide was composed of some greigite (Fe_3S_4) and mackinawite ($Fe_{1+x}S$), however, the bulk of the material at room temperature probably consists of disordered greigite and mackinawite. The weakly magnetic and strongly magnetic iron sulphide are good adsorbents for heavy metals and halogenated hydrocarbons.

Keywords: Sulphate-reducing bacteria; Iron sulphides; Nanoparticles; Magnetic properties; Structure

* Corresponding author.

0304-8853/00/$ - see front matter
PII: S0304-8853(00)00025-1

1. Introduction

In previous work on the precipitation of heavy metals by sulphate-reducing bacteria [4–7], it was shown that many metal ions in solution could be reduced from ppm levels to ppb levels and, if there were magnetic ions present, their precipitates onto the bacterial cell wall could make the microorganism sufficiently magnetic for removal from the suspension by high gradient magnetic separation (HGMS). A wide range of metal ions were treated in this way such as Ag, Hg, Pb, Cu, Zn, Sb, Mn, Fe, As, Ni, Sn, Al and other metals such as Rh, Au, Ru, Pd, Os, Pt, Cr were also removed. Many of the metals removed do not form insoluble sulphides but were removed when iron sulphide was produced. Watson and Ellwood [7] concluded that the bacterially produced iron sulphide was acting as an adsorbent for a wide range of heavy metals including many not normally precipitated as sulphides. Typically, the metal ion concentration was reduced from 10 ppm to a few ppb [1]. The capacity for heavy metals was 200–400 mg g of adsorbent. EXAFS studies [1] reveal that many of the metal ions were chemisorbed.

This paper examines the structure of the weakly magnetic and the strongly magnetic forms of iron sulphide produced by sulphate-reducing bacteria in order to increase the understanding of how the magnetic properties and how adsorption processes occur. First, the weakly magnetic material was examined using magnetic methods together with XANES and EXAFS spectroscopy. Second, the structure of the strongly magnetic iron sulphide is examined using EXAFS, XANES etc. Third, the question of the occurrence of strongly magnetic iron sulphides in nature is discussed in relation to the work described here.

2. Experimental methods and results

2.1. Properties of iron sulphides

To give a perspective it is necessary to review the known properties of iron sulphide in the compositional range of interest. The magnetic properties of the sulphides of iron are quite variable depending on the exact nature of the Fe/S ratio as shown by Schwarz and Vaughan [8]. The magnetic properties of the monoclinic pyrrhotite Fe_7S_8 were first examined over 75 years ago and the crystallographic, thermodynamic and magnetic aspects continue to be studied today.

At 50% Fe, the FeS is troilite, in which all Fe sites are individually magnetic and all the available sites for Fe are occupied. Troilite is antiferromagnetic below the Néel temperature $T_N = 325°C$. Between these two limits lies the region of the 'FeS', more accurately written $Fe_{1-x}S$. The generic pyrrhotite formula signifies iron cation vacancies and x varies from 0 to 0.13 and the magnetic susceptibility varies greatly [8]. The range of structural variants within this compositional region is quite complex. In addition to the ferrimagnetic monoclinic Fe_7S_8 ($x = 0.125$, 46.67 at% Fe), there are a variety of closely related hexagonal and monoclinic crystal structures which are linked to the number and spatial order or disorder of the Fe cation vacancies (which become mobile in the 200–300°C range). Randomly frozen vacancies produce hexagonal pyrrhotite which will be approximately antiferromagnetic. Ordered vacancies such as at Fe_7S_8 produce a monoclinic structure which is ferrimagnetic. (The saturation magnetisation value of 0.1 T is about one-fifth that of nickel.) At the chemical composition Fe_3S_4 a strongly ferrimagnetic material occurs, named griegite [9]. This material has the spinel structure. Ideally, for easy and cheap recovery of the adsorbent material from suspension, it is necessary for the microorganisms to produce either Fe_7S_8 or Fe_3S_4.

The redox potential, which controls the oxidation state of Fe, is critical for the production of the $Fe_{1-x}S$. The pH which controls the concentration of sulphide ions in solution $[S^{2-}]$ and the other anions and cations can also affect the magnetic properties of the material produced by the microorganisms and a small change in the composition can have a very large affect on the magnetic susceptibility of the $Fe_{1-x}S$ material.

If iron is present in the growth medium then iron sulphide will be precipitated on the cell wall of the bacterium. Depending on the circumstances, which will be discussed in more detail below, the material precipitated can be weakly or strongly magnetic.

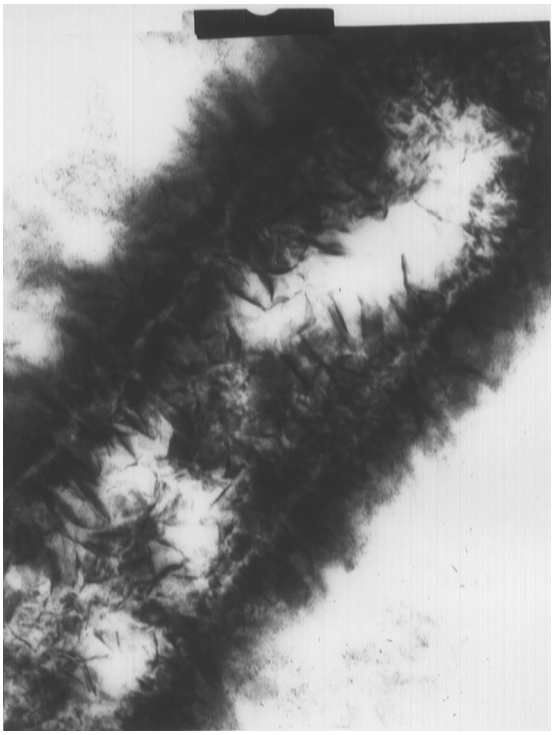

Photo 1. A transmission electron microscope micrograph of a longitudinal section through a sulphate-reducing bacterium. The bacterium is coated with a finely divided iron sulphide precipitate. The scale bar at the bottom of the plate is 1 mm in length.

Both materials look the same under the electron microscope at low magnification. Aqueous suspensions of iron sulphide (approximately 0.1 mg/ml) were ultrasonically dispersed and one drop of each suspension was deposited on a separate thin carbon film supported on a copper mesh TEM specimen grid. When thoroughly dried under nitrogen, these were examined in a JEOL.JEM 2000FX TEM operating at 200 kV accelerating voltage. Photo 1 shows a transverse view through a sulphate-reducing bacterium. This bacterium is approximately 0.8 μm in diameter and has a length of approximately 4 μm. A layer of precipitated iron sulphide, approximately 0.1 μm thick, can be seen around the surface. This material is finely divided and appears to consist of particles a few nanometres in diameter. At the top of the plate is iron sulphide that has become detached from the surface of the bacterium and this material, together with the microorganisms which produce it, collects as a sludge in the bottom of the bioreactor. The bacterium continues to metabolise even with a thick iron sulphide coating; this indicates that the iron sulphide must form an open structure through which nutrients can easily flow. This openness is very important when the material is used as an adsorbent as it ensures that the uptake of the adsorbate can be rapid.

2.2. Preparation of weakly magnetic iron sulphide

The adsorbent was produced using sulphate-reducing microorganisms in a 100 ml chemostat. The chemostat was first sterilised in an autoclave and then flushed with oxygen-free nitrogen and then isolated from atmospheric oxygen to establish and maintain anaerobic conditions. The temperature was maintained constant at 32°C by placing the chemostat in a water bath whose temperature was accurately controlled at 32°C. The medium used to culture the sulphate-reducing bacteria was Postgate's Medium C [10] modified by the addition of Fe sufficient to maximise the production of iron sulphide.

The medium was sterilised by filtration and the chemostat was first partly filled with the medium and then incubated with 20 ml of a culture of sulphate-reducing bacteria taken from a number of natural sources. After 24 h the medium was continuously added to the chemostat at a dilution rate of 0.1 h^{-1}. Large quantities of the weakly magnetic iron sulphide adsorbent were produced as a sludge and could be collected from the bottom of the chemostat for the adsorbent studies [7]. Measurements on the adsorbent showed that it contains 15% solids by weight of $Fe_{1-x}S$ with remainder being water.

2.3. Surface area measurements on the weakly magnetic material

The surface area of the freeze-dried material was measured using the BET method [11] and gave a value of 18.4 $m^2\ g^{-1}$.

It is clear from Photo 1 that the material in suspension, prior to drying, contains many nano-sized particles and, in consequence, it is expected

that the surface area of the material is greater than 18.4 $m^2\ g^{-1}$. The BET method cannot be applied without the sample being dried but an estimate of the surface area can be determined from the adsorption studies of metal ions onto the weakly magnetic material [1], as follows:

2.3.1. Cadmium

The highest concentration observed in these measurements was 0.97 mmol g^{-1} of adsorbent. The bonding behaviour of the adsorbed cadmium was determined using EXAFS; it was found to be chemisorbed to the surface of the iron sulphide forming bonds characteristic of the Wurtzite structure, an hexagonal form of cadmium sulphide. The characteristic length of the Cd–S bond was observed at 0.251 nm but also a Cd–Cd separation of 0.418 nm was also observed by EXAFS [1]. Assuming hexagonal packing, the area occupied per Cd ion is 0.1506 nm^2 so that the area over which cadmium is adsorbed as the Wurtzite structure is 84 $m^2\ g^{-1}$. This indicates that the total surface area is greater than or equal to 84 $m^2\ g^{-1}$.

2.3.2. Copper

The highest adsorbed concentration observed for copper was 2.18 mmol g^{-1} of adsorbent. The ion size for Cu^{2+} is very close to Fe^{2+} at 0.072 and 0.074 nm, respectively. A plausible way to estimate the surface area is to assume that all the defects, Fe^{2+} vacancies, become occupied by Cu^{2+}. Assuming that the composition is $Fe_{1-x}S$, the number of defects per unit volume, D_d, is $(xN_{A\rho})/[(1-x)A_w(Fe) + A_w(S)]$ where N_A is Avogadro's number, ρ is the density of the material, $A_w(Fe)$ and $A_w(S)$ are the atomic weights of Fe and S, respectively. The number of surface defects D_s is approximately $D_s = (D_d)^{2/3}$. For Fe_7S_8 with $x = 0.125$ and $\rho = 4.6$ [12], then $D_d = 4.3 \times 10^{27}\ m^{-3}$ and $D_s = 2.6 \times 10^{18}\ m^2$. Applying this result to the adsorption of Cu, the surface area of the adsorbent must be 504 $m^2\ g^{-1}$ of adsorbent, if all the defects are occupied. If all the defects are not occupied, the specific surface area must be larger.

This important topic will be readdressed in the discussion section when the results from the magnetic properties, EXAFS and neutron scattering can also be included in the evaluation of the surface area.

2.4. Preparation of strongly magnetic iron sulphide

The method described in this section is designed to produce a population of microorganisms which will produce a strongly magnetic product. The processing cost depends strongly on the magnetic properties of the materials [2] and it was desired to produce a product similar to Fe_7S_8 phase or Fe_3S_4, both of which are ferrimagnetic, in substantial quantities always remembering that the material must retain the adsorbent properties, as good or better than the weakly magnetic material.

In order to accomplish the task of making large quantities of strongly magnetic iron sulphide, Watson and Ellwood invented a new method [2]. In an extremely interesting paper, Freke and Tate [13] reported the almost complete removal of iron as insoluble sulphide from both ferrous and ferrous–ferric solutions and they found under certain, poorly specified conditions, i.e. microorganisms, redox potential E_h (although it appears E_h was very low) etc., the formation of substantial amounts of magnetic iron sulphide. Freke and Tate were never able to produce the magnetic material when the microorganisms were cultured in stirred batches. The problem seems to be that under a particular set of conditions produced by the composition of the solution to be treated, the microorganisms which produce the most magnetic product are outgrown by microorganisms with a less desirable product. This gave support to the idea that there are circumstances when strongly magnetic material can be produced [2,14].

In the method of Watson and Ellwood [2,14] progress towards the production of a more magnetic product was achieved in two steps. First, magnetically separating the output from the chemostat; the strongly magnetic particles of iron sulphide together with the microorganisms in intimate contact with the particles. Second, feeding this strongly magnetic fraction and the attendant microorganisms back to the chemostat or using this material to inoculate a new chemostat. Using this method it was possible to increase the strongly magnetic fraction from a few % to greater than

90% in a period of 3 months. At this point inocula taken from the chemostat were used to produce a consistent source of strongly magnetic iron sulphide.

The magnetic mineral was separated from the output of the chemostat by high gradient magnetic separation (HGMS) [15–17] in a field of 1 T. The remaining material was less magnetic and higher applied fields were needed to provide a higher force to extract the remaining material. At this moment further work is needed to understand how the population of the microorganisms in the chemostat has been changed during the application of magnetic feedback process described above.

The average chemical composition of the iron sulphide material is $Fe_{1-x}S$ where $x = 0.21$. The density of the sludge of magnetic sulphide as taken from the bottom of the chemostat in the form of a fine particulate suspension which is approximately 5% solids by weight. The actual density of the iron sulphide material is expected to be between 4.08 and 4.7 g cm^{-3} [12].

The wet strongly magnetic iron sulphide suspension can be freeze-dried forming a solid strongly magnetic iron sulphide with a density of 3.9 g cm^{-3}.

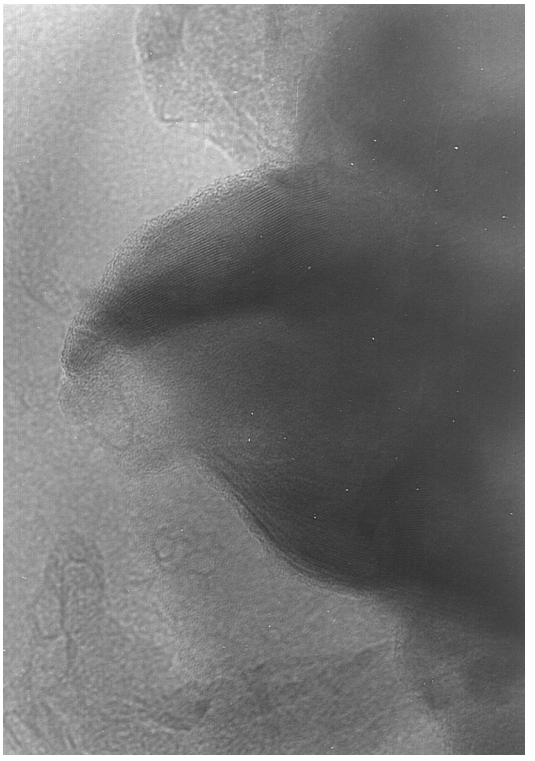

Photo 2. TEM micrograph at much higher magnification than 1. This reveals a material which in the main has no distinct morphology or clear grain boundaries.

3. The structural properties of the strongly magnetic iron sulphide

The structural properties of the strongly magnetic iron sulphide material have been examined in detail using transmission electron microscopy, surface area measurements, magnetic measurements, extended X-ray absorption fine-structure (EXAFS) spectroscopy and X-ray absorption near-edge structure (XANES) spectroscopy at Daresbury and neutron scattering at the ISIS facility of the Rutherford-Appleton Laboratory.

3.1. Transmission electron microscopy

The samples were prepared as described for Photo 1 but observations were carried out at higher magnification, as shown in Photo 2. The sample of magnetic iron sulphide consisted of very small, irregular particles or clusters of particles. The vast majority appeared entirely featureless with no clear grain boundary or distinctive morphology.

However, occasionally regions such as that shown in Photo 3 can be found. This micrograph shows an irregularly shaped domain, approximately 20×60 nm in size, in which lattice fringes can be seen which have a spacing of approximately 0.57 nm.

These fringes are not entirely straight, continuous or parallel to one another throughout the domain, but bend and terminate in edge dislocations in a fairly irregular way. The majority of particles, in which no lattice fringes are evident are either amorphous, or so poorly crystalline that there is insufficient coherent scattering throughout the thickness of the crystal (approximately 10–200 nm in electron-transparent regions) for lattice fringes to be visible, or they are oriented such that no prominent zone axes are parallel to the electron beam, or

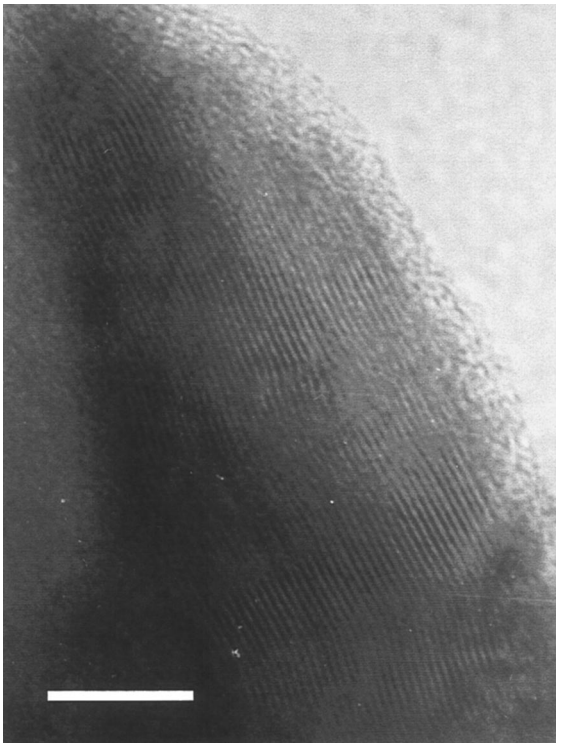

Photo 3. A crystalline area of strongly magnetic iron sulphide. The lattice spacing is approximately 0.57 nm. The white scale-bar is 10 nm long.

Photo 4. Selected area electron diffraction patterns (SAD) of the bacterially produced, strongly magnetic adsorbent material showing hexagonal arrays of spots and diffuse rings.

any suitably oriented lattice fringes are more closely spaced than can be resolved (approximately 0.2 nm). It should be remembered, however, that in the TEM only a minute fraction of the material is sampled and preferentially the lighter, smaller particles.

These observations in images are consistent with the corresponding selected-area electron diffraction (SAD) patterns, shown in Photo 4. Each pattern is produced from an area of specimen approximately 0.1 μm in diameter. Most such patterns indicate that the material is amorphous on this scale, i.e. there is little or no long- or intermediate-range order. (EXAFS spectroscopy and neutron scattering provide information on short-range order, in contrast to electron or X-ray diffraction.) However, a few areas produce weak, diffuse, continuous or spotty powder-type ring SAD patterns, indicating a poor degree of crystallinity with very small crystalline domains randomly oriented within the selected area. The lattice spacing of these rings are consistent with greigite [9,18], but the pattern is very weak and incomplete, so unequivocal identification as greigite is difficult. At first glance, the apparently single-crystal diffraction pattern (or patterns) consisting of spots in hexagonal array superimposed on the ring pattern would seem to suggest the presence of individual crystals with hexagonal or cubic symmetry. Careful measurement and calculation indicates that a hexagonal array of spots with this reciprocal lattice spacing could be produced if the crystal structure were hexagonal, viewed with an electron beam parallel to [0 0 0 1], with $\boldsymbol{a}$ approximately 0.3 nm, or if it were cubic, viewed along $\langle 1\ 1\ 1 \rangle$, with $\boldsymbol{a}$ approximately 0.37 nm. Neither of these possibilities closely matches any of the known Fe-sulphide structures in the JCPDS diffraction database. However, the

lattice parameters of the tetragonal iron sulphide mackinawite [19,20] are such that a ⟨1 1 1⟩ zone-axis section would fit the observed pattern reasonably well.

The superimposed SAD patterns, shown in Photo 4 (hexagonal array of spots and diffuse rings), suggest that the sulphide probably consists of an intimate mixture of greigite and mackinawite. In this small area mackinawite is present as one or two crystals, whereas the greigite seems to occur as an almost randomly oriented set of poorly formed, disordered crystalline domains. The image shown in Photo 2 probably shows one of the larger of such domains, with the 0.57 nm fringes corresponding to greigite (1 1 1) [9] lattice planes. Postfai et al. [21] have studied, by TEM, iron sulphides from magnetotactic bacteria collected from natural habitats. They have similarly observed that mackinawite and greigite coexist in their specimens and that the greigite is highly disordered. Mackinawite is unstable and they have found that it converts to greigite over time. The transformation of synthetic mackinawite to greigite has also been observed by Lennie et al. [22] by the application of heat and also after prolonged exposure to the atmosphere. Using the bacterium *Desulfovibrio desulfuricans* Canet 41, Rickard [23] was able to form iron sulphide material which was found to contain five iron sulphides, namely greigite Fe_3S_4, mackinawite $Fe_{1+x}S$, marcasite FeS_2, pyrite FeS_2 and pyrrhotite $Fe_{1-x}S$. Rickard also found that the magnetic component in the iron sulphide produced by Freke and Tate [13] also contained greigite and mackinawite. The XANES spectroscopy measurement of the material, discussed, indicates tetragonal symmetry is a strong feature and such a feature occurs in mackinawite.

3.2. Surface area measurements on the strongly magnetic iron sulphide

The surface area of the freeze-dried material was measured using the BET method [11] and gave a value of 18.4 $m^2\ g^{-1}$.

In order to compare the surface area of the weakly magnetic material with the strongly magnetic adsorption experiments were carried out with the strongly magnetic material with Cu and Cd for comparison with the earlier work [7]. Solutions with Cu were prepared containing metal ions at a concentration of 10 ppm at pH 6 which were shown to be stable with time.Various amounts of adsorbent were added then following the protocol outlined above [7] results were obtained for Cu, as follows:

1. Cu, initial concentration 10 ppm, with a concentration of strongly magnetic adsorbent of 100 ppm. The concentration of Cu remaining in solution after 390 min was 1.67 ppm (83.3% removal). This compared with a value of 1.7 ppm for the weakly magnetic adsorbent in the previous work [7]. Analysis method was ICP-MS.
2. Cu, initial concentration 10 ppm, with a concentration of strongly magnetic adsorbent of 100 ppm. The concentration of Cu remaining in solution after 300 min was 1.67 ppm (83.3% removal). This compared with a value of 1.8 ppm for the weakly magnetic adsorbent in the previous work [7]. Analysis method used AA for comparison with ICP-MS above.
3. Cu, initial concentration 10 ppm, with the concentration of the strongly magnetic adsorbent of 1000 ppm. The concentration of Cu remaining in solution after 300 min was < 0.03 ppm (99.7% removal). This compared with a value of also < 0.03 ppm for the weakly magnetic adsorbent in the previous work [7]. Analysis method was AA.

The results for Cd were as follows:

1. Cd, initial concentration 10 ppm, with the concentration of strongly magnetic adsorbent of 100 ppm. The concentration of Cd remaining in solution after 300 min was 0.62 ppm (93.8% removal). This compared with a value of 1.55 ppm for the weakly magnetic adsorbent in the previous work [7]. Analysis method was ICP-MS.
2. Cd, initial concentration 10 ppm, with the concentration of strongly magnetic adsorbent of 1000 ppm. The concentration of Cd remaining in solution after 270 min was 9.3 ppb (99.91% removal). This compared with a value of 0.10 ppb for the weakly magnetic adsorbent in the previous work [7]. Analysis method was ICP-MS.

The adsorption results for the weakly and the strongly magnetic materials for Cu and for Cd were so similar that there is a case for supposing the surface areas per g of the two materials are similar. This is supported by the magnetic flux-trapping measurements on the strongly magnetic material which allows an estimate of the adsorbent surface area to be made and is discussed in more detail below. This method was not possible for the weakly magnetic material which showed no flux trapping.

3.3. Magnetic properties of the strongly magnetic iron sulphide

From the studies of the strongly magnetic material using the electron microscope it is assumed that the sample consists of an intimate mixture of mackinowite which is diamagnetic and greigite which is ferrimagnetic. Both minerals occur in particles with a wide range of size. Larger particles of greigite were identified by their lattice spacing but the crystalline structure showed some disorder. Most of the material must be highly disordered so that the antiferromagnetic interaction between the electron spins must be weakened reflecting the disorder in the material.

The feedback chemostat was a device developed to increase the magnetic properties of the adsorbent and to investigate its action the following procedure was adopted. The magnetic component was separated from the outflow from the chemostat using a magnetic separator. These separators can operate with a variable background magnetic field. If the background magnetic field is weak then only the most strongly magnetic components are separated. If the background magnetic field is increased more weakly magnetic material can be collected. For the feedback chemostat to operate most efficiently a weak background field is used allowing only the very strongly magnetic material to be fed back to the chemostat. When the feedback chemostat was first operated with the starting material from the semi-saline source, only 4–5% of the strongly magnetic material was present and collected by the magnetic separator with a background field of 1 T. As time went on the percentage of the 1 T component increased. When the 1 T component reached 17% of the material passed through the separator the material passing through the separator was re-separated at a field of 2 T and a further 21% was separated. After a further few weeks of the feedback process the 1 T component reached 54% so that it is of interest to measure this material with the material being produced at an earlier stage and the magnetisation versus applied magnetic field for these components at a temperature of 290 K are shown in Figs. 1a and b. The notation to refer to the samples, is that the earlier sample, collected after 1 month is denoted by A an the later sample collected after 2 months, is denoted by B. The samples in Figs. 1a and b are 'A17% 1 T', 'A 21% 2 T' and 'B 50% 2 T'.

Fig. 1a shows the magnetisation at low applied magnetic field for three components of the material from the feedback chemostat. The 1 T components both showed hysteresis at low field. The hysteretic part appeared to saturate at 0.5 T when the magnetisation became linear with increasing field in both cases and as shown in Fig. 1b, the linearity persisted to 10 T, the limit of the measurements. Using the density of greigite as 4080 kg m^{-3} given by Spender et al. [24], the susceptibilities of the linear regions were about $\chi = 6 \times 10^{-4}$ for the 'B 54% 1 T' material and 7.2×10^{-4} for the 'A 17% 1 T' material. It seems reasonable that the hysteretic regions are due to the large particles identified as greigite by the electron microscope; but because the 'B 50% 1 T' sample contained a greater fraction of greigite than the 'A 17% 1 T' sample means that the actual susceptibilities in the linear regions for 'A 17% 1 T' and 'B 50% 1 T' are much closer than the values quoted above. It appears that the linear regions must be caused by the amorphous material in which the spin–spin interaction has been weakened so much by disorder that the spins are decoupled at 290 K and the material behaves like a paramagnet. The 'A 21% 2 T' material shows no low-field hysteresis and is paramagnetic with $\chi = (1.1) \times 10^{-4}$.

Spender et al. [24] have measured the magnetisation of greigite and find that the magnetic moment corresponds to $2.2 \pm 0.03\ \mu_B$ per formula weight which, for a paramagnetic material, corresponds to $\chi = (3.1) \times 10^{-3}$. One interpretation is that the spin density of the amorphous material is the same as greigite and then the volume fractions of the

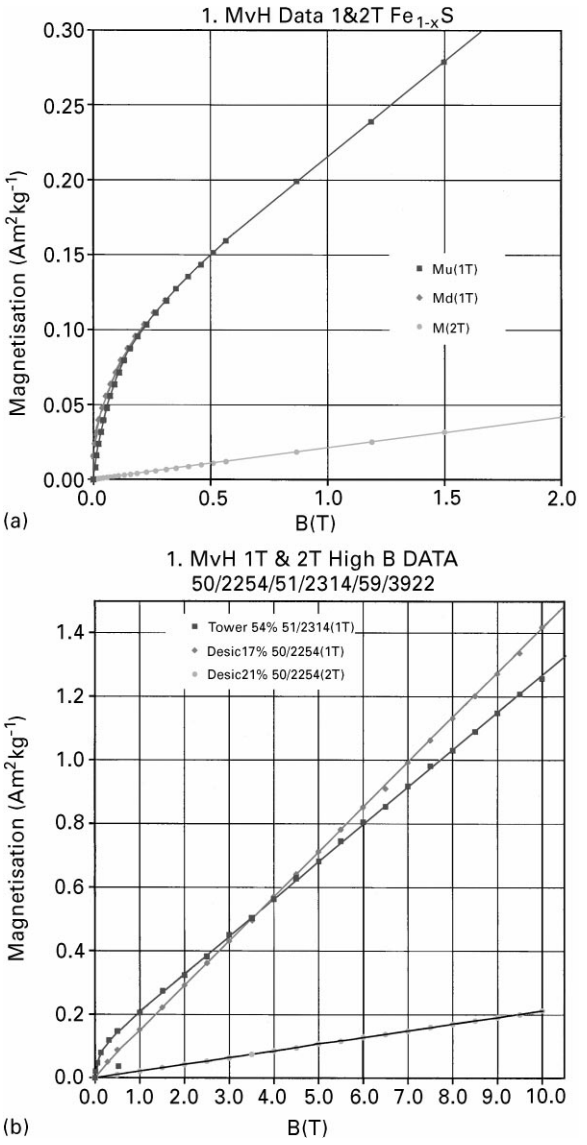

Fig. 1. (a) The magnetisation M (amp m^2 kg^{-1}) versus field B (T) for the iron sulphide adsorbent sample 'B 54% 1 T' and Mu(1 T) and Md(1 T) are the magnetisation versus applied field for increasing field and for decreasing field, respectively. This sample shows hysteresis below 0.2 T. The magnetisation of the sample 'A 21% 2T' (labelled M(2 T)), showed no hysteresis. The measurements were performed at 290 K. (b) Shows the magnetisation versus applied magnetic field for the samples 'A 17% 1 T', 'B 50% 1 T' and the ' A 21% 2 T'. The maximum applied field was 10 T and at this field the magnetisation samples was linear in field and showed no indication of saturation.

amorphous greigite would be 0.18, 0.23 and 0.04 for the 'B 54% 1 T' material, the 'A 17% 1 T' material and the 'A 21% 2 T' material, respectively. The remainder of the material would be amorphous mackinowite.

A sample of FeS produced by sulphate-reducing bacteria, under unspecified conditions, has been reported by Coe et al. [25] which shows similar behaviour to the 1 T samples in Fig. 1b. The sample is magnetic with $\chi = (3.17) \times 10^{-4}$ in the linear region which approximately a factor of 2 smaller than the 1 T materials reported here.

As feedback proceeded over a period of 3 months the fraction of 1 T component increased to approximately 90% but also the paramagnetic components became more strongly magnetic with material not captured at 5 T, the so-called non-magnetic material, reaching $\chi = (1.1) \times 10^{-4}$ which is similar to the 'A 21% 2 T' sample shown in Figs. 1a and b.

These materials, as revealed by the microscope pictures, contained greigite; the surface area estimates and their strongly magnetic nature, suggest that these materials are composed of particles of small enough to be single domain at low enough temperature and superparamagnetic at higher temperature. However, at 290 K, the magnetisation curves in Figs. 1a and b suggest that thermal effects disrupt the long-range coupling between spins so that the material is not superparamagnetic but paramagnetic.

To further elucidate the nature of these materials a series of experiments were carried out to investigate flux trapping in the materials. The samples were obtained by HGMS from batch B, as follows:

The material collected by HGMS with a background field of 0.5 T amounted 20% of the total and was labelled as 'B 20% 0.5 T'. The material which passed through the separator with a background field of 0.5 T was passed through the separator again with a background field of 5 T when a further 34% was retained; this material was labelled 'B 50% 5 T'. The material which passed through at 5 T was labelled 'B 50% > 5 T'. The samples were magnetised with a field of 5 T at a temperature of 5 K and when the field was switched off they showed considerable trapped magnetisation, as shown in Fig. 2a. When the

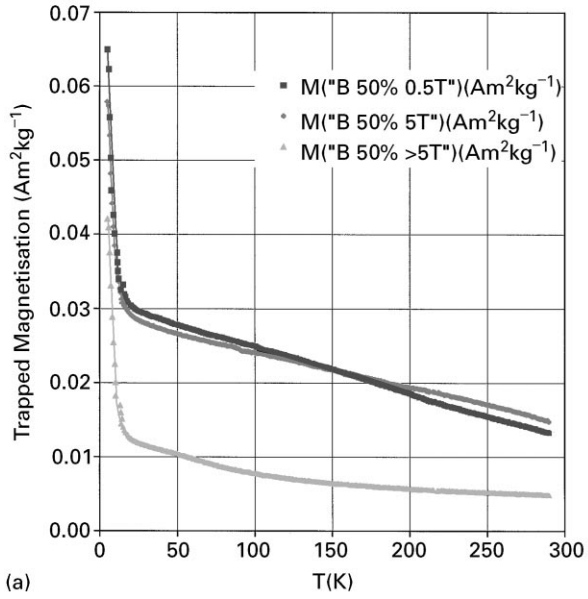

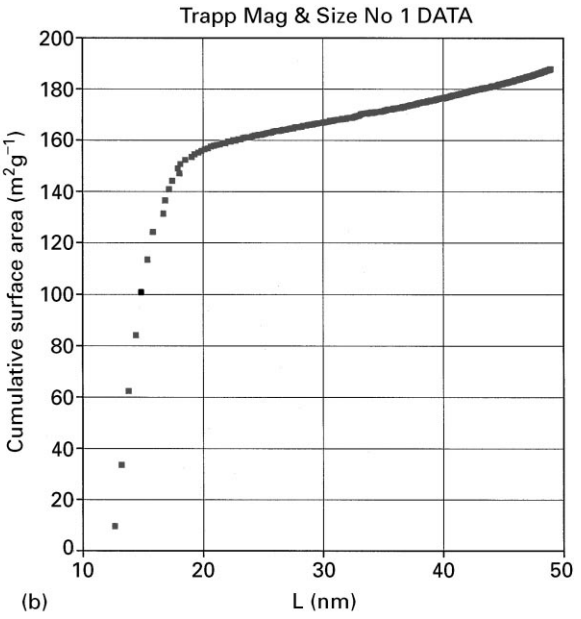

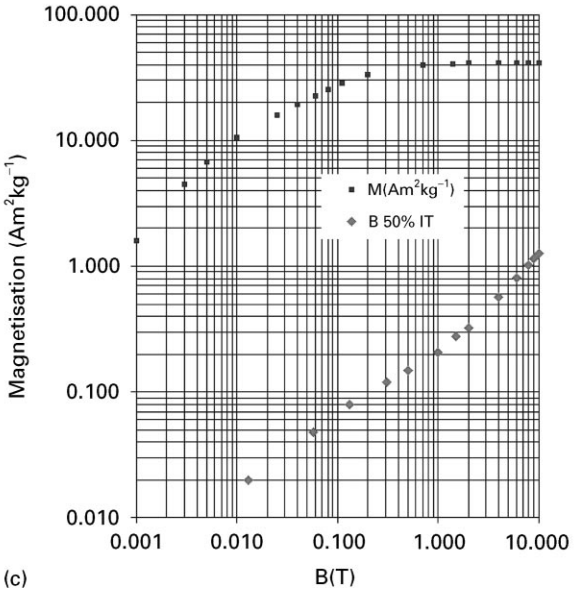

Fig. 2. (a) The trapped magnetism in the strongly magnetic 'B 50% 0.5 T', 'B 50% 5 T' and 'B 50% $>$ 5 T' samples as a function of temperature. The sample was first cooled to 5 K from 290 K in field of 5 T. At 5 K the applied magnetic field was turned off and the trapped magnetisation was measured as a function of temperature as the temperature was slowly raised. (b) The accumulated surface area obtained using the data in Fig. 2a for 'B 20% 0.5 T' is plotted versus particle length L (nm) (assuming that $q = 3$) using $K = 3788$ J m^{-3}, $f_0 = 10^{10}$ s^{-1} and $\tau = 1$ s. The contribution of the superparamagnetic part to the magnetisation in the presence of the trapped field was not included. It must be remembered that there may be a further large contribution to the surface area from material whose blocking temperature is less than 5 K. (c) The magnetisation versus applied field (upper curve) calculated using Eq. (2) for a single-domain system with the particle-size distribution determined from the data shown in Fig. 2a and assuming a value of 17.6 μ_B per unit cell (determined for greigite by Spender et al. [24]). For comparison the lower curve is the measured values of the magnetisation at 290 K for a 'B 50% 1 T' sample, also shown in Fig. 1b. It is clear that the curves are very different in shape confirming that the single-domain model is inadequate at 290 K.

samples were slowly warmed, all samples measured showed a large drop in magnetisation between 5 and 20 K followed by a slow decrease of trapped magnetisation as the temperature increased to 290 K. The samples 'B 20% 0.5 T' and 'B 50% 5 T' were very similar but the sample 'B 30% >5 T' trapped considerably less magnetisation than the other two samples. The most likely explanation is that the sample contains appreciably less strongly magnetic material than the other samples. If the difference were due to the fact that the particle size in this sample is less than the others then it would be expected that may show a higher trapped flux at 5 K but this is not the case. These results suggest that these materials at lower temperature than 290 K contain single-domain particles and superparamagnetic particles above their blocking temperature [26,27] and at high enough temperature becoming paramagnetic.

The fall in magnetisation between 5 and 20 K, produced by particles becoming unblocked, indicates that a large fraction of the crystallites are of the order of a few nanometres in size. However, in order to evaluate the results of flux trapping in more detail, the properties of single-domain particles must be examined.

The magnetic nature of single-domain particles have been examined by Brown [26]and by Aharoni [28]. They showed that the magnetic properties are determined by the anisotropy energy (KV) of the crystallites with volume, V, and where, K, is the anisotropy energy per unit volume and contains contributions from a number of sources. For anisotropy energies $KV > k_b T$ where k_b is the Boltzmann constant and T is the temperature, the magnetisation of the crystallites, for the uniaxial case, is restricted to the easy axis and is in one direction or the opposite direction. Thermal effects produce transitions between these two directions so that the average lifetime τ between the switching processes is given by

$$1/\tau = f_0 \exp(-E_B/k_b T), \tag{1}$$

where E_B is the energy barrier between the two directions and may contain contributions from crystalline anisotropy, surface and shape anisotropy, f_0 is some frequency, for example the natural frequency of gyromagnetic precession, often taken to be $10^{10}\,s^{-1}$. These processes were examined [26,28] in the absence of an applied magnetic field so that $E_B = KV$. The theory was extended by Aharoni [29] to include the effects produced by a magnetic field B. In the presence of an applied field B, $E_B = KV - \mu B$ where μ is the magnetic moment of the particle. If the single-domain distribution $F(V)$ can be determined as the fraction of particles with volume V, then the magnetisation M versus applied field can be calculated and is given by

$$M = n_p \sum F(V)\mu(V) L_g(\mu(V)B/k_b T), \tag{2}$$

where n_p is the number of particles per unit volume, $F(V)$ is the fraction of particles of volume V, $\mu(V)$ is the magnetic moment of a particle of volume V and $L_g(\mu(V)B/k_b T)$ is the Langevin function given by $L_g(\mu B/kT) = \coth(\mu(V)B/kT) - 1/(\mu(V)B/kT)$, which is appropriate when $\mu(V) \gg \mu_b$, the Bohr magneton.

For small values of $\mu(V)B/k_b T$, $L_g \approx$ constant so that in order to account for the linearity of M versus B up to 10 T as shown in Fig. 1b M, within the single-domain model, must be dominated by small values of μ and therefore by small values of V. This will be discussed more fully below when an estimate of $F(V)$ has been made.

Diaz Ricci and Kirschvink [30] have examined greigite produced within intracellular organelles (magnetosomes) and have calculated the boundaries for the onset of superparamagnetism and single-domain and double-domain behaviour for parallelepipeds. They used the form for K given by Néel [31] as $K = M_s H_c/32\pi^2$ where M_s is the saturation magnetisation and the fine particle coercive force H_c is given by $H_c = 4\pi(N_t - N_p)M_s$ where N_p and N_t are demagnetisation factors parallel to and transverse to the length, respectively, and where $N_p + 2N_t = 1$. As the temperature increases larger particles become unblocked, some remaining blocked at 290 K, which accounts for the hysteresis observed at low field in the graph of magnetisation versus field, as shown in Fig. 1a. The largest particle observed with the electron microscope was 20×60 nm, assuming the particle was 20 nm thick, gives a volume V of $V = 2.4 \times 10^{-23}\,m^3$ and an aspect ratio q(length L/width) = 3. With the aspect ratio $q = 3$ then $N_t - N_p = 0.395$ [32]. Assuming

this particle is blocked at 290 K gives a value of $K \approx 4000\ \mathrm{J\,m^{-3}}$. However, a more accurate estimate can be obtained by using K due to Néel [31] discussed above. Using the values of $M_s = 1.69 \pm 0.24 \times 106\ \mathrm{A\,m^{-1}}$ [24] and $H_c = 1054 \pm 0.200\ \mathrm{mT}$ gives a value of $K = 7.088 \pm 0.84 \times 10^3\ \mathrm{J\,m^{-3}}$. Then with $f_0 = 10^{-10}\ \mathrm{s^{-1}}$ and $\tau = 1$ s gives a domain of length 49 ± 9 nm with $q = 3$ as the boundary between single domain and superparamagnetic behaviour and clearly shows that the largest observed crystalline region is a single domain particle are blocked at 290 K. This value of $L = 49 \pm 9$ nm is consistent the value of $L = 44$ nm given by Diaz Ricci and Kirschvink [30] who chose a value of $K = 10^4\ \mathrm{J\,m^{-3}}$ which best fitted their results overall and value of $J_s (= M_s/4\pi) = 1.23 \times 10^5\ \mathrm{A\,m^{-1}}$ which at $q = 3$ gives a value of $N_t - N_p > 1$, suggesting that K should be smaller and/or M_s larger than the values Diaz Ricci and Kirschvink use.

The quantity H_c usually called the microscopic coercivity and is the value that would be measured at 0 K but there are at least two processes which can reduce H_c. First, at finite temperature thermal fluctuations can reduce the value of the coercivity to H_B which has been given by Néel [33] and discussed by Evans and McElhinny [34]

$$H_B = H_c - 4\pi((Q + \ln \tau) 2 k_b T H_c / (M_s L^3 / q^2))^{1/2}, \quad (3)$$

where Q has a numerical value of about 22 [33], and, as above, with $t = 1$ s, $H_c = 1.054$ T, $M_s = 2.12 \times 106\ \mathrm{A\,m^{-1}}$, $L = 50$ nm and $q = 3$ gives a value of $H_B = 53 \pm 20$ mT. Measurements of the materials discussed here using the methods described by Roberts [18] gave a value for $H_B = 50$ mT which is consistent with the calculated value of 53 mT described above.

A second process which can reduce the coercive force is the interaction between grains. This interaction depends on the size and shape of the grains and their distance apart and is very difficult to calculate. However, the effect is revealed by asymmetric hysteresis loops produced by an AC magnetic field [35,36].

Under a large externally applied field the magnetisation reaches a saturation value M_s and when the field is switched off the magnetisation M falls to M_R where $M_R = M_s/2$ for the case of uniaxial symmetry. For synthetic greigite, Spender et al. [24] found a value of 0.43 ± 0.02 which, although 14% smaller than the value of 0.5 expected for uniaxial symmetry, it is considerably smaller than the values for cubic anisotropy of 0.831 or 0.866 given by Wohlfarth [37]. More recently in 21 samples of greigite from different sources, Roberts [18] has found an average value of 0.44 ± 0.1.

When $E_B < k_b T$ the value of τ becomes small and thermal processes drive the magnetic moment which then follows a random motion, with the magnetic moment of each particle $M_s V \gg \mu B$, the Bohr magneton, characteristic of superparamagnetism [27]; the particles do not contribute to the trapped magnetic moment but can contribute to the magnetisation in the presence of a trapped field.

Using the value of the anisotropy energy from Diaz Ricci and Kirschvink [30] obtained by assuming $q = 3$ and the value of the saturation magnetisation found by Spender et al. [24], the trapped magnetism versus temperature in Fig. 2(a) was used to determine a particle size distribution and assuming the trapped magnetic fields have little influence on the blocking temperature [29]. Aharoni [29] has examined the effect of a magnetic field on the relaxation time. For uniaxial symmetry the two directions for the magnetisations now have different energies depending whether the scalar product $(M_s \cdot H)$ is positive or negative. Further the energy barrier E_B can be changed. To investigate these problems, Aharoni introduced two parameters $h = BM_s/2K$ and $\alpha = KV/k_b T$; here B is the applied field $(T)(M_s\ \mathrm{A\,m^{-1}})$, in the case discussed here the field produced by the trapped magnetisation, and k_b is the Boltzmann constant. At 5 K the magnetic field produced in the sample by the trapped magnetisation is 4.5 mT which gives a value of $h = 0.008$ and $\alpha = 23$. Aharoni suggests for these values of h, f_0 is constant to about 10% in Eq. (1). It is also assumed that the magnetic interaction between grains is small and K is independent of temperature and q is constant at $q = 3$ and independent of the particle volume $V = L^3/q^2$.

The particle-size distribution provides an estimate of the surface area of the adsorbent and the magnetisation versus applied magnetic field can be calculated using Eq. (2).

The accumulated surface area obtained using the data in Fig. 2b is plotted versus particle length

L (nm) (assuming that $q = 3$). The value of K was assumed to be constant, independent of V, at $3788\ \mathrm{J\,m^{-3}}$. The contribution of the superparamagnetic part to the magnetisation produced by the trapped field was not included. The results indicated that 25% of the trapped magnetism remained in blocked particles at 290 K. The results indicate that the surface area of the material which becomes unblocked above 5 K is $190\ \mathrm{m^2\,g^{-1}}$, which is about a factor of 2 smaller than the area estimated by the adsorption of the heavy metals described above. As shown in Fig. 2a the trapped magnetism increases rapidly with decrease temperature, and the surface area increases very rapidly as the particle size reduces. This implies that a considerable contribution to the surface area comes from particles which are already unblocked and superparamagnetic at 5 K.

As mentioned above, the particle size distribution can be used to calculate the magnetisation distribution using Eq. (2). This magnetisation curve has been calculated and is shown in Fig. 2c. In Fig. 2c, the curve calculated from Eq. (2) is displayed with the measured magnetisation curve of sample 'B 54% 1 T' shown in Fig. 1b as can be seen a calculation based on superparamagnetism cannot explain the linear region of the magnetisation versus applied magnetic field observed. The majority of the material is paramagnetic but as the temperature is lowered below 290 K, the material must progressively become superparamagnetic and finally single-domain material as the temperature decreases. This allows flux trapping to occur.

4. Extended X-ray absorption fine structure (EXAFS)

4.1. Experimental details

The FeS sample was prepared and loaded into Perspex sample holders with Sellotape windows in Southampton. Data were collected at ambient temperature in the transmission mode on station 9.2 of the Daresbury Synchrotron Radiation Source (SRS), operating at 2 GeV with an average current of 150 mA. A Si(2 2 0) double-crystal monochromator was used, detuned to reject 50% of the incident signal in order to minimise harmonic contamination. The monochromator angle was calibrated for the Fe spectrum by running an edge scan for a Fe foil. Io and It were measured using ion chambers filled with a mixture of Ar/He. Two scans were recorded at the Fe K-edge for this sample and the spectra of the iron sulphide model compounds were collected in transmission mode on station 7.1 of the SRS using a Si(1 1 1) double-crystal monochromator, detuned to 50% rejection.

The isolated EXAFS data were analysed using EXCURV92 [38], employing the exact spherical wave calculation [39,40]. Phase shifts were derived from ab initio calculations using Hedin–Lundqvist potentials and von Barth ground states [41]. The theoretical fits were obtained by adding shells of backscattering atoms around the central absorber atom and iterating the Fermi energy, E_f, the absorber–scatterer distances, r, and the Debye–Waller factors, $2\sigma^2$, to minimise the sum of the square of the residuals between the experiment and the theoretical fit. The numbers of scatterers, N, in each shell were chosen as the integer values that gave the best fit. Only shells which made a significant improvement to the R-factor were included in the final fit. The R-factor in the tables is a measure of the goodness of fit, defined by the equations:

$$R = \sum_i (1/\sigma_i)(|(\text{experiment}(i) - (\text{theory}(i)|) \times 100\%,$$

where

$$1/\sigma_i = k(i)^3/\sum_j (k(j)^3)(|\text{experiment}(j)|).$$

5. Experimental results

5.1. XANES spectroscopy

The X-ray absorption near-edge structure (XANES) of the Fe K-edge spectrum is compared in Fig. 3 with the XANES of several iron sulphide model compounds. The sharp pre-edge feature and the structure on the edge of the magnetic iron sulphide material most closely resembles that of mackinawite, in which the Fe is tetrahedrally coordinated to four S atoms [42]. The absence of a peak

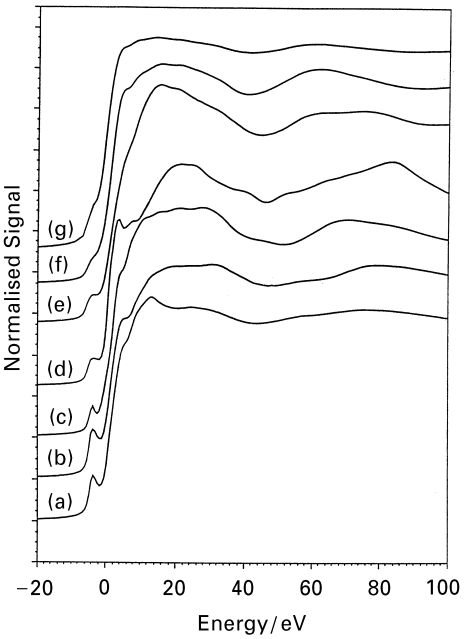

Fig. 3. XANES spectra of the magnetic iron sulphide and model compounds. (a) Strongly magnetic iron sulphide, (b) mackinawite, (c) bornite, (d) pyrite, (e) greigite, (f) weakly magnetic iron sulphide and (g) troilite.

Table 1
Three fits to the Fe K-edge EXAFS data for bacterially produced weakly magnetic iron sulphide, showing the effect on the *R*-factor of adding outer shells, where *r* is the distance between the central (Fe) atom and the scatterer, $\pm$ 0.02 Å and $2\sigma^2$ is the Debye–Waller $\pm$ 20%. The values of *r* were determined using X-ray crystallography for hexagonal pyrrhotites by Keller-Besrest and Collin [3,43]

Shell	*r* (Å)[a]	*r* (Å)	$2\sigma^2$ (Å^2)	*R*-factor
2 × S	2.37	2.39	0.02 1	38.41
4 × S	2.55	2.67	0.044	
4 × Fe	2.95	2.96	0.052	
4 × Fe	3.73	3.82	0.050	
2 × Fe	4.18	4.09	0.041	
10 × Fe	~ 4.6	4.85	0.045	
2 × S	2.37	2.39	0.021	43.14
4 × S	2.55	2.67	0.044	
4 × Fe	2.95	2.96	0.052	
4 × Fe	3.73	3.82	0.050	
2 × Fe	4.18	4.09	0.041	
2 × S	2.37	2.40	0.020	48.87
4 × S	2.55	2.67	0.040	
4 × Fe	2.95	2.96		0.057

[a] Keller-Besrest, [3], # 384, 385.

before the main absorption edge indicates the Fe is in sites with octahedral symmetry [42]. In greigite one-third of the Fe sites have tetrahedral coordination with the other two-thirds showing octahedral coordination.

5.2. EXAFS spectroscopy

5.2.1. Weakly magnetic iron sulphide

The k^3-weighted Fe K-edge EXAFS spectrum and best fit of the magnetic iron suulphide and the corresponding Fourier transforms are shown in Fig. 4.

Table 1 shows three fits the Fe K-edge EXAFS data for bacterially product weakly mangetic iron sulphide.

5.2.2. Strongly magnetic iron sulphide

The Fe K-edge EXAFS spectrum of the iron sulphide contains contributions from more than one shell of backscatterers, and displays several distinct peaks in the Fourier transform (Figs. 4a and b). The main peak, at ca. 2.2 Å, corresponds to a shell of sulphur scatterers around the central iron atom. The best fit is with 3 S atoms at 2.23 Å. The EXAFS signal giving rise to the peak in the Fourier transform at ca 3.4 Å cannot be fitted with a single shell of Fe or S scatterers, and the best fit is with a shell of 2 Fe atoms at 3.16 Å and a shell of 2 Fe atoms at 3.57 Å. The small peak in the Fourier transform at ca 2.8 Å can best be fitted with a shell of 1 S atom at 2.77 Å. There is a contribution to the spectrum at ca. 2 Å, which is best fitted with a shell of 1 O atom. Figs. 5(a) and (b) show the best fit to the experimental spectrum and the associated Fourier transforms. Table 2 lists the fitting parameters for the best fit, together with other fits for comparison.

5.2.3. Discussion of the EXAFS results

The XANES profile (Fig. 3) and the EXAFS fitting parameters (Table 2) clearly show that the Fe is mainly tetrahedrally coordinated. Tetragonal symmetry is revealed in XANES by the small peak at a lower energy than the main adsorption edge

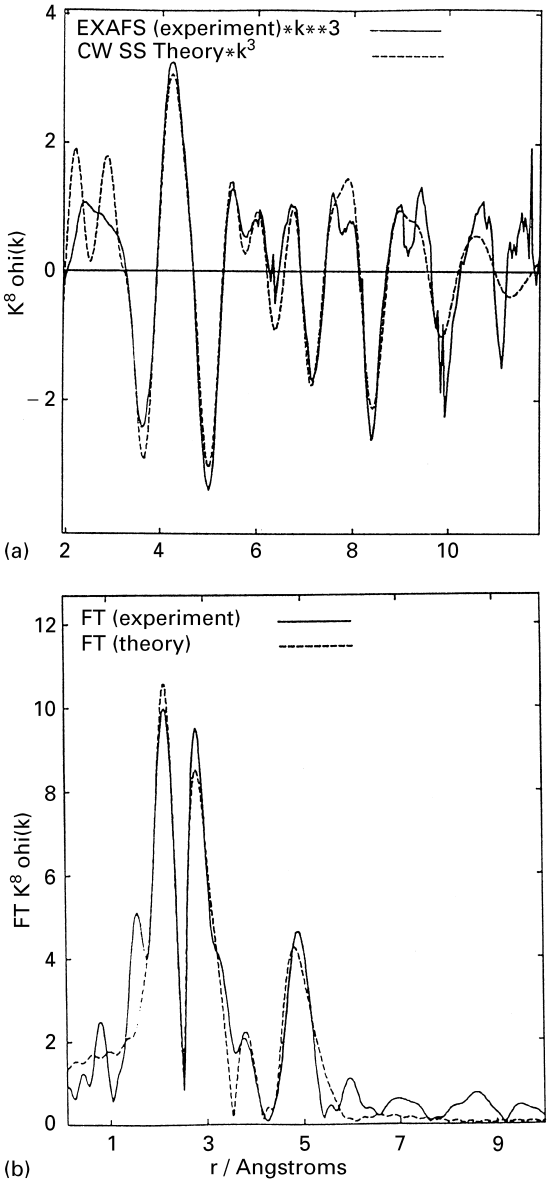

Fig. 4. (a) The k^3-weighted Fe K-edge EXAFS spectrum (solid line) and best fit (broken line) of the magnetic iron sulphide, and (b) the corresponding Fourier transforms.

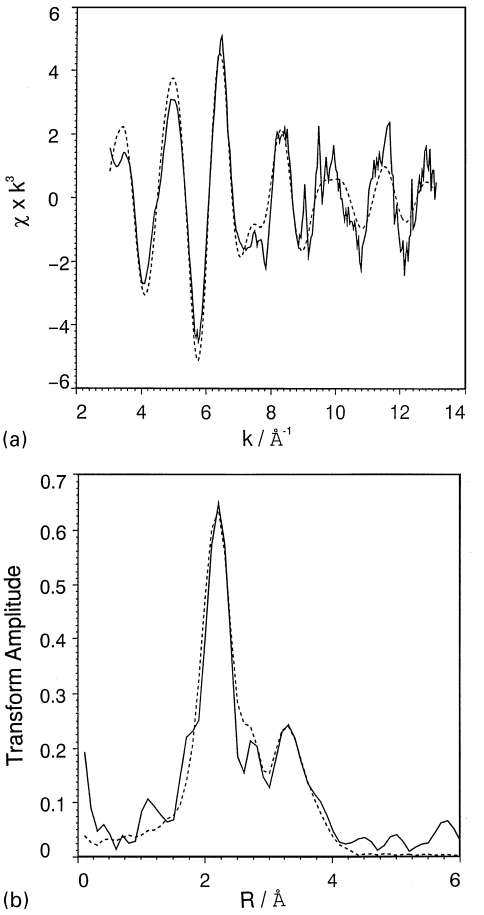

Fig. 5. (a) The k^3-weighted Fe K-edge EXAFS spectrum (solid line) and best fit (broken line) of the magnetic iron sulphide, and (b) the corresponding Fourier transforms.

[42]. This is consistent with a mixture of mackinawite and greigite which is suggested by electron diffraction. The Fe in mackinawite is completely tetrahedrally coordinated whereas in greigite only a third of Fe is in tetrahedral coordination. The greigite is strongly magnetic whereas mackinawite is weakly diamagnetic indicating that a substantial fraction of the material is greigite. The best fit is with 3 S atoms and 1 O atom, implying that there may be some oxidation of the iron, particularly at the surface of the sample.

5.2.4. Neutron scattering data for the magnetic iron sulphide

Preliminary neutron scattering data was obtained for freeze-dried magnetic iron sulphide at the ISIS Facility at the Rutherford-Appleton Laboratory. The neutrons are pulsed; each pulse contains neutron wavelengths λ between 0.1 and 4 Å. The

Table 2
The best fit (lowest *R*-factor) and the effect of adding further shells to the Fe K-edge EXAFS data for bacterially produced strongly magnetic iron sulphide for the shells centred on an Fe atom where *r* is the distance between the central (Fe) atom and the scatterer, ± 0.02 Å and $2\sigma^2$ is the Debye–Waller $\pm 20\%$

Shell	*r* (Å)	$2\sigma^2$ (Å^2)	*R*-factor
1 × O	2.13	0.00 9	25.4
3 × S	2.19	0.01 7	
1 × S	2.77	0.01 1	
2 × Fe	3.16	0.02 3	
2 × Fe	3.56	0.029	
1 × S	2.08	0.061	28.9
2 × S	2.22	0.01 2	
1 × S	2.76	0.011	
2 × Fe	3.15	0.023	
2 × Fe	3.55	0.029	
3 × S	2.23	0.020	37.1
1 × S	2.77	0.01 1	
2 × Fe	3.16	0.02 2	
2 × Fe	3.57	0.031	
3 × S	2.23	0.02 0	40.9
1 × S	2.65	0.026	
2 × Fe	3.17	0.025	
2 × Fe	3.59	0.031	

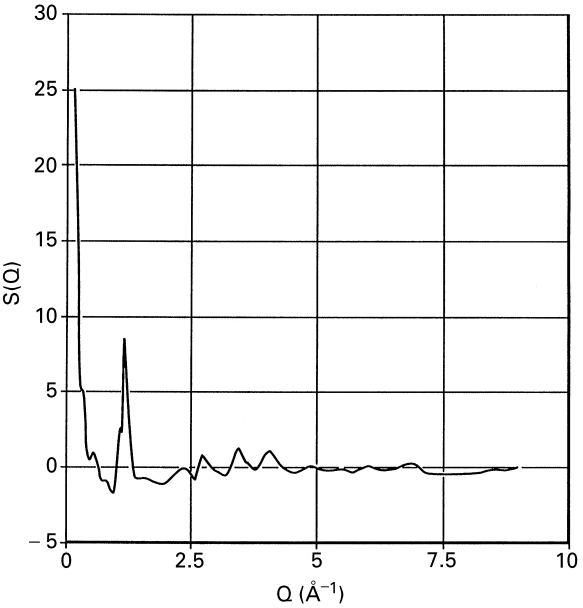

Fig. 6. The structure factor $S(Q)$ plotted versus Q, the momentum transfer, for the freeze-dried magnetic iron sulphide, obtained using the pulsed neutron source at the ISIS facility, Rutherford Appleton Laboratory, UK.

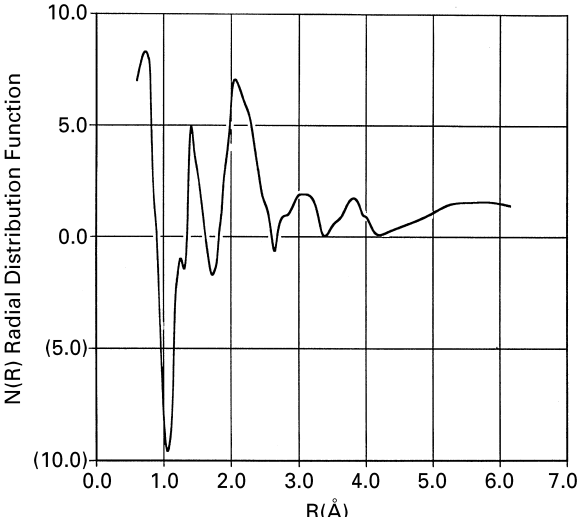

Fig. 7. The radial distribution function $N(R)$ plotted versus distance R(Å). $N(R)$ is obtained as a Fourier transform of $S(Q)$.

neutrons were detected by 1000 detectors between the scattering angles between 5 and 30°. The momentum transfer Q, is given by $Q = 4\pi \sin\theta/\lambda$ where θ is the angle through which the neutrons of wavelength λ are scattered. The structure factor $S(Q)$ is the sum of the neutron counts received at a momentum transfer Q. As shown in Fig. 6, $S(Q)$ shows some interesting features. At very low Q, $S(Q)$ rises rapidly as Q decreases indicating that very small particles are present. The radial distribution function shows oscillations beyond 20 Å so that it is possible that the sample, rather than consisting of 20 Å particles in diameter, is a porous material containing 20 Å holes. It is difficult to distinguish between these two cases with the present preliminary data.

The radial distribution function, shown in Fig. 7, has a pronounced negative peak near $r = 1$ Å, indicative of OH bonds. The main feature is a strong Bragg peak near 2.1 Å^{-1} with other peaks at 2.98 and 3.8 Å^{-1} but as yet no interpretation has been found, but the peak at 2.1 Å^{-1} correlates well with the lattice spacing of 5.7 Å observed by TEM.

5.2.5. Discussion of neutron scattering results

A plausible explanation, based on the magnetic measurements, the stability against oxidation even in the presence of gaseous oxygen together with the neutron scattering data, suggests that during the freeze-drying process the material collapses forming a porous material composed of small magnetic particles of iron sulphide 2–3 nm in diameter with holes of average diameter of the order of 2 nm between the particles. The surface area of the material, as suggested by the measurements of trapped magnetic flux, should be of the order of 400–500 $m^2\ g^{-1}$. As mentioned above, the surface area of the freeze-dried material was measured by the BET method [11] as 18.4 $m^2\ g^{-1}$ which is less than the estimates of the area of the material prior to freeze-drying as $> 550\ m^2\ g^{-1}$ from adsorption of heavy metals [1] and similar values estimated from the transmission electron microscope pictures [7] and from neutron scattering measurements, described above.

The surface area for the freeze-dried measured using the BET method gave a value of 18.4 $m^2\ g^{-1}$ which indicates most of the pores 20 Å pores are inaccessible to nitrogen gas, used in the BET method, which means the pores are blocked off.

However, in the material which has not been freeze-dried a large fraction of small particles must provide a large surface area onto which the adsorption of metal ions occurs. The weakly magnetic materials have been shown to adsorb a wide range of heavy metals [1] and from this the surface area must be of the order of 400–500 $m^2\ g^{-1}$.

Watson and Ellwood [7] concluded that the bacterially produced iron sulphide was acting as an adsorbent for a wide range of heavy metals including many not normally precipitated as sulphides. Typically, the metal ion concentration was reduced from 10 ppm to a few ppb [1]. The capacity for heavy metals was 200–400 mg g of adsorbent. EXAFS studies [1] reveal that many of the metal ions were chemisorbed.

6. Discussion and conclusions

Sulphate-reducing bacteria occur widely in anaerobic sedimentary environments such as rivers, estuaries, harbours, salt marshes, lakes, canals and the deep sea. These bacteria are responsible for many large iron sulphide deposits. Magnetic iron sulphides have been reported from many sedimentary environments. Magnetotactic bacteria usually produce magnetosomes containing single-domain particles of magnetite (Fe_3O_4) and single-domain greigite (Fe_3S_4) particles are also known. It has often been suggested that magnetic components of sediments are due to the remains of magnetotactic microorganisms. However, these microorganisms are notoriously difficult to grow in the laboratory and they are comparatively rare in nature compared with sulphate-reducing bacteria. We conclude that perhaps we have been reproducing a process which can occur, in exceptional circumstances, in natural anaerobic sediments and which may be almost entirely responsible for the appearance of the observed magnetic iron sulphides, both strongly and weakly magnetic material. These iron sulphide materials are produced by sulphate-reducing bacteria as a consequence of their metabolism, if they are situated in a solution containing iron. The strong adsorption for a wide range of metal ions we have observed in these bacterially produced iron sulphides suggest that materials produced in sediments would be relatively impure and the impurities may consist of considerable amounts of material not normally precipitated as sulphides whereas the material produced in magnetosomes would be relatively pure.

Further, perhaps the presence of this extremely effective natural heavy metal immobilisation process widely occurring in anaerobic sediments must mitigate to a great extent releases of many metals into the environment. It may also be possible and profitable to engineer releases of these metals into the environment to take full advantage of these naturally occurring processes and we suggest that this will be a very fruitful area of investigation for environmental engineers.

Acknowledgements

The authors wish to acknowledge the provision of time on DARTS, the UK national synchrotron radiation service at the CLRC Daresbury

Laboratory and ISIS, the pulsed neutron facility at the Rutherford-Appleton Laboratory. We are grateful to Prof. D.J. Vaughan and Dr. R.A.D. Pattrick of the Department of Earth Sciences, Manchester University, for making available the XANES spectra of the iron sulphide model compounds. We also wish to thank colleagues at University of Southampton for useful discussions, namely, Professor Brian Rainford and Drs George Attard, Ian Croudace, Peter de Groot, Alan Howard, Patrick James and P. Warwick. We also wish to acknowledge financial support from Biopraxis Developments Ltd., the Office of Innovation and Research Support at University of Southampton, Southampton Innovation Ltd and NSG Environmental Ltd.

References

[1] J.H.P. Watson, D.C. Ellwood, Q. Deng, S. Mikhalovsky, C.E. Hayter, J. Evans, Minerals Eng. 8 (1995) 1097.
[2] J.H.P. Watson, D.C. Ellwood, C.J. Duggleby, Minerals Eng. 9 (1996) 973.
[3] F. Keller-Besrest, G. Collin, J. Solid State Chem. 84 (1990) 211.
[4] J.H.P. Watson, D.C. Ellwood, IEEE Trans. Magn. MAG-23 (1987) 3751.
[5] J.H.P. Watson, D.C. Ellwood, A biomagnetic separation process for the removal of heavy metal ions from solution, Presented at International Conference on Control of Enviromental Problems from Metal Mines, Roros, Norway, 1988.
[6] D.C. Ellwood, M.J. Hill, J.H.P. Watson, Pollution control using microorganisms and magnetic separation, Presented at Microbial Control of Pollution, University of Cardiff, Cardiff, Wales, 1992.
[7] J.H.P. Watson, D.C. Ellwood, Minerals Eng. 7 (1994) 1017.
[8] E.J. Schwarz, D.J. Vaughan, J. Geomag. Geoelectr. 24 (1972) 441.
[9] B.J. Skinner, R.C. Erd, F.S. Grimaldi, The Am. Minerol. 49 (1964) 543.
[10] J.R. Postgate, The Sulphate-reducing Bacteria, 2nd edition, Cambridge University Press, Cambridge, England, 1984.
[11] S. Brunauer, P.H. Emmett, E. Teller, J. Am. Chem. Soc. 60 (1938) 309.
[12] L.F. Power, H.A. Fine, Minerals Sci. Eng. 8 (1976) 106.
[13] A.M. Freke, D. Tate, J. Biochem. Microbiol. Tech. Eng. 3 (1961) 29.
[14] J.H.P. Watson, D.C. Ellwood, Feedback chemostat, British Patent Application, Vol. GB 9516753.2, 1995.
[15] J.H.P. Watson, J. Appl. Phys. 44 (1973) 4209.
[16] J. Svoboda, Magnetic Methods for the Treatment of Minerals, 1st Edition, Vol. 8, Elsevier, Amsterdam, 1987.
[17] P.G. Marston, J.J. Nolan, L.M. Lontai, US Patent, pp. No. 3 627 678, 1971.
[18] A.P. Roberts, Earth Planetary Sci. Lett. 134 (1995) 227.
[19] H.T. Evans Jr, C. Milton, E.C.T. Chao, I. Adler, C. Mead, B. Ingram, R. A. Berner, Valleriite and the new iron sulphide, mackinawite, US Geological Survey Professional Papers, Vol. 475-D, 1964, pp. 64–69.
[20] A.R. Lennie, S.A.T. Redfern, P.F. Schofield, D.J. Vaughan, Mineral. Mag. 59 (1995) 677.
[21] M. Postfai, P.R. Buseck, D.A. Bazylinski, R.B. Frankel, Am. Mineral 83 (1998) 1469.
[22] A.R. Lennie, S.A.T. Redfern, P.E. Champness, C.P. Stoddart, P.F. Schofield, D.J. Vaughan, Am. Mineral. 82 (1997) 302.
[23] D.T. Rickard, Stockholm Contributions Geol. 20 (1969a) 50.
[24] M.R. Spender, J.M.D. Coey, A.H. Morrish, Canadian J. Phys. 50 (1972) 2313.
[25] B.T. Coe, R. Gerber, D. Witts, IEEE Trans. Magn. 34 (1998) 2126.
[26] W.F. Brown Jr., Phys. Rev. 130 (1963) 1677.
[27] I.S. Jacobs, C.P. Bean, Fine particles, thin films and Exchange Anisotropy, in: G.T. Rado, H. Suhl (Eds.), Magnetism-Spin Arrangements and Crystal Structure, Domains and Micromagnetics, Vol. III, Magnetism, Academic Press, New York, 1963, pp. 271–350.
[28] A. Aharoni, Phys. Rev. 135 (1964) A447.
[29] A. Aharoni, Phys. Rev. 177 (1969) 793.
[30] J.C. Diaz Ricci, J.L. Kirschvink, J. Geophys. Res. 97 (1992) 17309.
[31] L. Néel, Adv. Phys. 4 (1955) 191.
[32] R.M. Bozorth, Ferromagnetism, 1st edition, D. Van Nostrand, New York, 1951.
[33] L. Néel, Ann. Geophys. 5 (1949) 99.
[34] M.E. Evans, M.W. McElhinny, J. Geomagn. Geoelectr. 21 (1969) 757.
[35] F. Preisach, Zeitschrift Phys. 94 (1935) 277.
[36] D.J. Dunlop, J. Geomagn. Geoelectre. 17 (1965) 459.
[37] E.P. Wohlfarth, J. Phys. 20 (1959) 295.
[38] N. Binstead, J.W. Campbell, S.J. Gurman, P.C. Stephenson, EXCURV92, Daresbury, Warrington, Daresbury Laboratory, England, 1991.
[39] P.A. Lee, J.B. Pendry, Phys. Rev. B 11 (1975) 2795.
[40] S.J. Gurman, N. Binstead, I. Ross, J. Phys. C 17 (1984) 143.
[41] L. Hedin, S. Lundqvist, Solid State Phys. 23 (1969) 1.
[42] G.A. Waychunas, M.J. Apted, G.E. Brown Jr., Phys. Chem. Minerals 10 (1983) 1.
[43] F. Keller-Besrest, G. Collin, J. Solid State Chem. 84 (1990) 194.